

# Hot accretion flow in black hole binaries: a link connecting X-rays to the infrared

Alexandra Veledina<sup>1</sup>, Juri Poutanen<sup>1</sup> and Indrek Vurm<sup>2,3</sup>

<sup>1</sup>*Astronomy Division, Department of Physics, PO Box 3000, FIN-90014 University of Oulu, Finland*

<sup>2</sup>*Racah Institute of Physics, Hebrew University of Jerusalem, 91904 Jerusalem, Israel*

<sup>3</sup>*Tartu Observatory, 61602 Tõravere, Tartumaa, Estonia*

2 October 2012

## ABSTRACT

Multiwavelength observations of Galactic black hole transients have opened a new path to understanding the physics of the innermost parts of the accretion flows. While the processes giving rise to their X-ray continuum have been studied extensively, the emission in the optical and infrared (OIR) energy bands was less investigated and remains poorly understood. The standard accretion disc, which may contribute to the flux at these wavelengths, is not capable of explaining a number of observables: the infrared excesses, fast OIR variability and a complicated correlation with the X-rays. It was suggested that these energy bands are dominated by the jet emission, however, this scenario does not work in a number of cases. We suggest here an alternative, namely that most of the OIR emission is produced by the extended hot accretion flow. In this scenario, the OIR bands are dominated by the synchrotron radiation from the non-thermal electrons. An additional contribution is expected from the outer irradiated part of the accretion disc heated by the X-rays. We discuss properties of the model and compare them to the data. We show that the hot flow scenario is consistent with many of the observed spectral data, at the same time naturally explaining X-ray timing properties, fast OIR variability and its correlations with the X-rays, which were not possible to understand within the jet paradigm.

**Key words:** accretion, accretion discs – black hole physics – radiation mechanisms: non-thermal – X-rays: binaries

## 1 INTRODUCTION

Although the black hole X-ray binaries (BHB) have been intensively studied for over four decades, many problems remain unsolved. Among the most debated topics are the physics of state transitions, the interplay between the cold accretion disc and the hot medium, the role of the jet, the source of rapid variability, radiative processes shaping the broadband spectrum and, specifically, the nature of various components contributing to its different parts. When addressing the latter problem, three distinct components are usually considered: the standard (or irradiated) cool accretion disc, the hot inner flow (or corona) and the jet. Their relative contribution depends on the spectral energy range and varies with time and can be assessed by performing (quasi-) simultaneous multiwavelength observations.

Over the past decade, numerous multiwavelength campaigns have resulted in a significant progress in the field. Broadband, radio to X-ray, spectral energy distributions (SEDs) for many BH sources were constructed (e.g. Hynes et al. 2000; McClintock et al. 2001; Chaty et al. 2003; Cadolle Bel et al. 2007, 2011; Durant et al. 2009). In addition to the spectral information, data on the fast variability are now available in the X-rays as well as at lower energies in the optical, infrared (OIR) and ultra-violet bands. The light

curves at lower energies are significantly correlated with the X-rays (Kanbach et al. 2001; Hynes et al. 2003, 2006, 2009b; Durant et al. 2008, 2009; Gandhi et al. 2010), showing a complex shape of the cross-correlation function. It provides an important information on the interrelation between various components and gives clues to their physical origin.

The radio emission in BHBs is likely dominated by the jet as supported by the observed linear polarization at a 1–3 per cent level in the hard state (Corbel et al. 2000) and up to ten per cent in spatially resolved components during the transient events (Fender et al. 1999; Hannikainen et al. 2000). In addition, a relatively high luminosity, requiring the size exceeding the typical binary separation (Fender 2006), as well as the detection of superluminal motion (Mirabel & Rodríguez 1994) lean towards this interpretation. The power-law-like radio spectrum is often attributed to synchrotron emission of an inhomogeneous source in analogy with the extragalactic jets (Blandford & Königl 1979). In blazars, the jet is also responsible for the X-ray and  $\gamma$ -ray production (Königl 1981; Dermer & Schlickeiser 1993; Sikora et al. 1994; Stern & Poutanen 2006). On the contrary, the jets in BHBs are unlikely to be responsible for bulk of the X-ray photons (for compre-

hensive discussion see Poutanen & Zdziarski 2003; Zdziarski et al. 2003).

The spectra of hard-state BHBs constitute a power-law in the X-ray band with a stable spectral slope and ubiquitous sharp cut-off at  $\sim 100$  keV (Gierlinski et al. 1997; Zdziarski et al. 1998; Ibragimov et al. 2005). It is broadly accepted to be produced by thermal Comptonization (e.g. Poutanen 1998; Zdziarski & Gierliński 2004). Additionally, a Compton reflection feature originating from cool opaque matter (likely the cool accretion disc) is often detected. Its strength is correlated with the X-ray slope (Zdziarski et al. 1999, 2003), with the width of the iron line as well as with the quasi-periodic oscillation (QPO) frequency (Gilfanov et al. 1999; Revnivtsev et al. 2001; Gilfanov 2010). These observations support a view that the X-rays are produced in the very vicinity of the BH, in a hot flow surrounded by the cold disc. In this scenario, variations in the mass accretion rate are correlated with the cool disc truncation radius (Poutanen et al. 1997; Esin et al. 1997), with the flux of soft seed photons that determines the spectral slope and with the reflection amplitude that scales with the solid angle the cold disc is seen from the hot flow. Correlations with the QPO frequency are also naturally explained, if the oscillations are produced in the innermost part of the accretion flow by Lense–Thirring precession (Ingram & Done 2011). Such a scenario would favour models, where seed photons for Comptonization are provided by the standard Shakura & Sunyaev (1973) accretion disc. However, the hot flow itself also produces synchrotron radiation that can contribute or even dominate the seed photon flux to the Comptonizing medium (Ghisellini et al. 1998; Wardziński & Zdziarski 2000, 2001; Poutanen & Vurm 2009; Malzac & Belmont 2009; Sobolewska et al. 2011; Veledina et al. 2011b).

Discovery of the high-energy (MeV) tails in the hard-state accreting BHBs (McConnell et al. 1994, 2002; Ling et al. 1997; Droulans et al. 2010; Jourdain et al. 2012) suggests the presence of non-thermal particles in these systems. Such particles may be produced in a hot inner flow or a jet. Their association with the jet, however, is inconsistent with detections of even more prominent high-energy non-thermal tails in the soft state of BHBs (Grove et al. 1998; Gierliński et al. 1999; Zdziarski et al. 2001; McConnell et al. 2002; Gierliński & Done 2003), when the jet is quenched (Fender et al. 2004). Thus, the hot accretion flow remains the only alternative. In the hard state, the entire X/ $\gamma$ -ray hard-state spectra can be produced by hybrid (thermal plus non-thermal) electrons via synchrotron self-Compton (SSC) mechanism (Poutanen & Vurm 2009; Malzac & Belmont 2009). The thermal part of the particle distribution is responsible for the power-law-like continuum with the sharp cut-off, while the non-thermal particles both produce seed synchrotron photons for Comptonization and contribute to the MeV energies via inverse Compton process. Transition to the soft state can then be associated with the rising role of the disc as a source of seed photons, which increase Compton cooling and cause changes in the electron distribution from mostly thermal to nearly non-thermal (Poutanen & Coppi 1998; Poutanen & Vurm 2009; Veledina et al. 2011b). The SSC mechanism was also shown to be consistent with the peculiar optical variability, which in a number of BHs in low-mass X-ray binaries (LMXBs) is partially anticorrelated with the X-ray emission (Kanbach et al. 2001; Durant et al. 2008; Gandhi et al. 2008). Namely, the increasing mass accretion rate results in a higher X-ray and a lower synchrotron OIR emission, because of an increasing role of synchrotron self-absorption within the source (Veledina et al. 2011a).

The OIR spectra of LMXBs often show an excess above the standard accretion disc (e.g., Hynes et al. 2000, 2002; Gelino et al. 2010). In some cases the spectrum can be described by a power-law of index close to zero (i.e.  $F_\nu \propto \nu^0$ ). Such data were previously explained by additional contribution from the irradiated disc (Gierliński et al. 2009), dust heated by the secondary star (Muno & Mauerhan 2006) or the jet (Hynes et al. 2002; Gallo et al. 2007). We show that they also can be explained by the synchrotron radiation from the non-thermal particles in the hot flow. However, in some cases the OIR fluxes are higher than expected from any candidate alone (Chaty et al. 2003; Gandhi et al. 2010), suggesting contribution of at least two components simultaneously. This can be a reason for the complex shape of the optical/X-ray cross-correlation function (Veledina et al. 2011a).

The general shape of the time-averaged X/ $\gamma$ -ray spectrum of BHB can be well explained in terms of a one-zone hybrid Comptonization model. However, the short-term spectral variability, reflected in hard X-ray time-lags (Miyamoto & Kitamoto 1989; Nowak et al. 1999a) and asymmetries of the cross-correlation function between hard and soft X-ray energy bands (Priedhorsky et al. 1979; Nolan et al. 1981; Maccarone et al. 2000), suggests that a number of regions simultaneously contribute to the total spectrum. The observed logarithmic dependence of the time-lags on photon energy can be phenomenologically explained by spectral pivoting (Poutanen & Fabian 1999). Theoretical model capable of explaining the observed timing properties was proposed by Kotov et al. (2001) and further investigated in Arévalo & Uttley (2006). It assumes that the X-ray spectrum is produced in the hot corona, present in a range of radii, by Comptonization of the disc photons. The power-law slope of the locally emitted spectrum depends on the distance from the BH: the hardest spectra are produced in the innermost region due to the lack of photons from the cold disc. The main source of the short-term variability in BHs is believed to be fluctuations in the mass accretion rate, propagating through the hot accretion flow (Lyubarskii 1997). The hard time-lags thus naturally appear from the perturbations propagating from the larger distances to the vicinity of the BH. The model of Kotov et al. (2001) considers thermal Comptonization of the disc photons, but as we show below the results hold in the framework of hybrid Comptonization, with the synchrotron mechanism as the major seed photon supplier.

It is clear, that the complete description of the timing and spectral properties of BHB requires a multi-zone model. In this paper we construct such a model for the extended hot accretion flow. This model is somewhat analogous to the inhomogeneous synchrotron models developed for extragalactic jets (Marscher 1977; Blandford & Königl 1979). The difference is that in our model the emission originates from an inflow, not an outflow. The advantage of the hot flow model is that the energy input can be estimated from the available gravitational energy transferred to particles via some mechanism, while in the jet scenario the energy release is an arbitrary function.

Similarly to the previously studied one-zone models (Poutanen & Vurm 2009; Malzac & Belmont 2009; Veledina et al. 2011b), we assume that gravitational energy is dissipated in the flow and is injected in the form of electrons having a power-law distribution. We compute the steady-state particle and photon distributions self-consistently by solving corresponding kinetic equations. Our aim is to understand the broadband spectral as well as timing properties of such a flow, and compare it to the BHB data.

In Section 2, we give constraints on the size of the hot accretion flow that can be derived from the observed level of the OIR emission. We first construct an analytical model for the hot flow as-

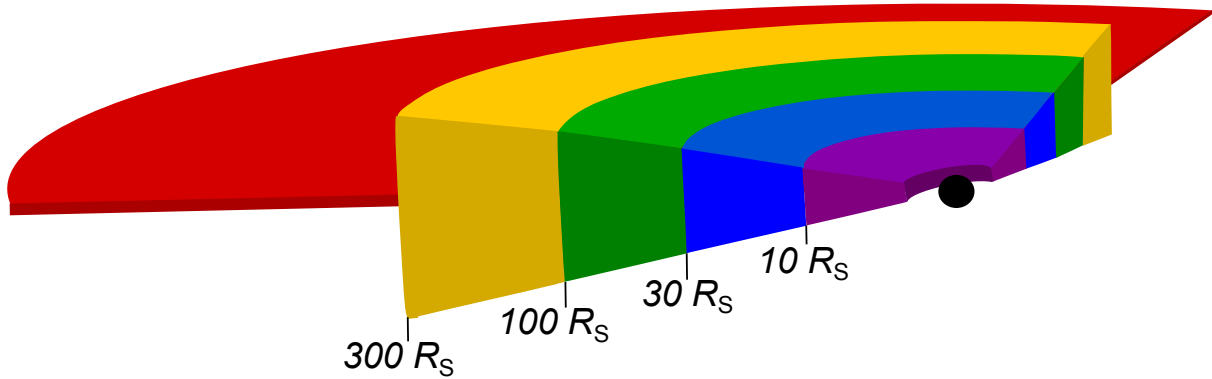


**Figure 1.** Schematic picture of the accretion flow inner regions. Red outer component represents the multi-color cold accretion disc, truncated at 300 Schwarzschild radii ( $R_S$ ). The inner parts are occupied by a geometrically thick hot accretion flow. In our numerical model, we split the inner hot flow into four zones with outer radii  $10R_S$  (violet),  $30R_S$  (blue),  $100R_S$  (green) and  $300R_S$  (yellow).

suming power-law dependences of the main parameters on radius. We then proceed to the numerical model where the electron distributions and the emitted spectra are computed self-consistently. In Section 3, we present the results of simulations for the model corresponding to the hard state of BHBs. We show that the multi-zone hot disc model produces flat OIR spectra resulting from synchrotron emission of non-thermal electrons at different radii. We model then the state transitions by decreasing the truncation radius of the hot flow. In Section 4, we provide a detailed analysis of the observational data and compare them to our model and to the jet scenario. We summarize our finding in Section 5.

## 2 ANALYTICAL MODEL

### 2.1 Geometry

Many observational properties suggest that the standard disc in the hard state is truncated far away from the central object (for detailed description and challenges to the truncated disc scenario, see review by Done et al. 2007). The inner part is probably occupied by some type of geometrically thick, optically thin, hot accretion flow, which is responsible for the X-ray Comptonization continuum, but also contributes to the longer wavelengths. One can roughly estimate the minimum size of the source that is required to produce the observed OIR luminosity.

Let us first assume that OIR emission is produced by thermal particles. The typical temperature of the electron gas determined from the Comptonization cut-off is  $kT_e \sim 100$  keV and the typical IR luminosity at 1 eV can reach  $\nu L_{\nu, 1 \text{ eV}} = 10^{36}$  erg s $^{-1}$ . Thus, we get the minimum size from the Rayleigh-Jeans formula

$$R = \left( \frac{\nu L_\nu}{8\pi^2 \nu (\nu/c)^2 kT_e} \right)^{1/2} \approx 2.3 \times 10^9 \text{ cm}. \quad (1)$$

For a  $10M_\odot$  BH, assumed in all calculations hereafter, this corresponds to  $750 R_S$  (here  $R_S = 2GM/c^2$  is the Schwarzschild radius). However, many observed properties (e.g. iron line width, amplitude of Compton reflection, drop of the iron line equivalent width with the Fourier frequency, see Gilfanov 2010) suggest that the cold disc in the hard state is truncated at a smaller radius. Thus, if the hot flow lies within the truncation radius, its thermal radiation is unlikely to be a good candidate to produce enough OIR photons.

However, even a weak, energetically unimportant non-thermal tail, in addition to the mostly Maxwellian distribu-

tion, gives a significant rise to the synchrotron luminosity (e.g. Wardziński & Zdziarski 2001). For example, a tail containing only one per cent of total particle energy increases it by a factor of 100. Accurate calculations (see below) show that the source size of  $R \approx (30 - 50)R_S$ , an order magnitude smaller than given by equation (1), would in principle be enough to radiate the observed OIR luminosity. Such a size is consistent with the above estimates of the truncation radius and with the typical size of the region of the gravitational energy release. It is worth noticing that a strong synchrotron emission from non-thermal particles makes it a good candidate for seed photons for Comptonization (Poutanen & Vurm 2009; Malzac & Belmont 2009), which implies that the SSC spectrum extends from the X-rays down to the OIR band with the low-energy turnover determined by the maximum extent of the hot flow.

### 2.2 Hard-state OIR spectra

Spectral properties of the hot flow in the OIR band can be understood from simple analytical considerations. Let us consider the flow with a constant height-to-radius ratio  $H/R$  ratio, extending between radii  $R_{\text{in}}$  and  $R_{\text{out}}$  (see Fig. 1 for the geometry). In order to estimate the synchrotron luminosity and spectra, we assume that the electrons follow a power-law distribution in Lorentz factor  $n_e(\gamma) \equiv dn_e/d\gamma = n_0 \gamma^{-p}$ , starting from  $\gamma_{\text{le}} = 1.0$ . Deviations from the power-law at low energies do not play any role, as the synchrotron emission produced by these electrons is self-absorbed. The Thomson optical depth across the disc is assumed to follow the power law  $\tau(R) \propto R^{-\theta}$ . For the constant  $H/R$  this is equivalent to  $n_0(R) \propto \tau/R \propto R^{-\theta-1}$ . We further assume that the magnetic field depends on the distance from the BH as  $B(R) \propto R^{-\beta}$ .

Our analytical model of the hot flow is analogous to the non-uniform synchrotron source models, previously applied to the emission from extragalactic jets (Condon & Dressel 1973; de Bruyn 1976; Marscher 1977; Blandford & Königl 1979; Königl 1981; Ghisellini et al. 1985). For the parameters considered here, most of the luminosity is produced in the inner part of the source, so that the OIR spectrum is composed of emission components coming from different radii and is not dominated by the radiation from the outer regions (these two cases are illustrated in figs 2a and 2b in Ghisellini et al. 1985).

A region of the disc at a given radius emits synchrotron radiation, which is self-absorbed below the turn-over frequency

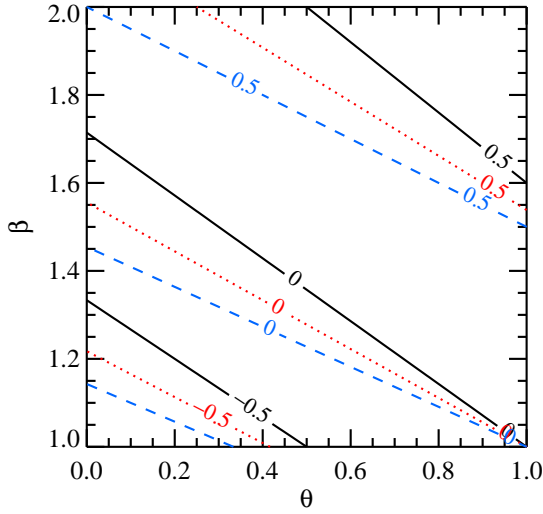


**Figure 2.** Contour plot of the index  $\alpha_{\text{OIR}}$  as a function of parameters  $\beta$  and  $\theta$  for three values of electron index  $p=2$  (solid black), 3 (dotted red) and 4 (dashed blue).

$\nu_t$ . For power-law electrons, this frequency can be calculated as (Rybicki & Lightman 1979; Wardziński & Zdziarski 2001)

$$\nu_t^{\text{pl}} = 3^{\frac{p+1}{p+4}} 2^{-\frac{6}{p+4}} \pi^{\frac{1}{p+4}} \nu_L^{\frac{p+2}{p+4}} [G_1(p) c R r_e n_0]^{\frac{2}{p+4}}, \quad (2)$$

where  $\nu_L = eB/(2\pi m_e c)$  is the Larmor frequency,  $G_1(p) \simeq 1$  is a combination of Euler's Gamma functions (due to averaging over electron pitch angles),  $r_e$  is the classical electron radius. Substituting the constants, we get

$$\nu_t^{\text{pl}} \approx 3 \times 10^{15} B_6^{\frac{p+2}{p+4}} (\sigma_T n_0 R)^{\frac{2}{p+4}} \text{ Hz}, \quad (3)$$

where  $Q = 10^x Q_x$  in cgs units. The term in brackets can also be written as  $\sigma_T n_0 R = \tau(\gamma_t) \gamma_t^p$ , with  $\gamma_t$  being the Lorentz factor of the electrons emitting at the turn-over frequency. In the later representation, the equation is also valid for hybrid electrons (e.g., Maxwellian with power-law tail), as long as the electrons emitting at the turnover frequency are in the power-law tail. The low-frequency cut-off for synchrotron spectrum from power-law electrons scales as

$$\nu_t \propto R^{-(\beta(p+2)+2\theta)/(p+4)}. \quad (4)$$

Again, for hybrid electron distribution one should consider scaling with radius of the power-law tail (parameter  $\theta$ ), which can be different from scaling of the total optical depth. As immediately follows from equation (3), the turn-over frequency may fall to optical and even IR wavelengths for sufficiently low magnetic field and/or Thomson optical depth.

The emission at the turn-over frequency is optically thick, so the intensity is equal to the source function for the power-law electrons. For isotropic electrons the intensity is (averaged over pitch angles)

$$I_{\nu_t} = \frac{m_e G_2(p)}{2\sqrt{3}} \nu_L^{-1/2} \nu_t^{5/2}, \quad (5)$$

where  $G_2(p) \simeq 1$  (again, coming from the angle-averaging). At each wavelength, there is a contribution from the optically thick and optically thin emission from different radii. For simplicity, we assume that emission from each radius contributes only to its own

turn-over frequency,<sup>1</sup> therefore the resulting spectrum of an inhomogeneous synchrotron source constitutes a power-law

$$\nu L_\nu = 4\pi^2 R^2 \nu I_\nu \approx 2 \times 10^{36} R_8^2 B_6^{-1/2} \nu_{15}^{7/2} \text{ erg s}^{-1}. \quad (6)$$

Substituting the appropriate parameter scaling and using equation (4), we get the spectral index

$$\alpha_{\text{OIR}} = \frac{5\theta + \beta(2p+3) - 2p - 8}{\beta(p+2) + 2\theta}, \quad (7)$$

where  $L_\nu \propto \nu^\alpha$ . In a wide range of parameters  $\beta \in [1, 2]$  and  $\theta \in [0, 1]$  the resulting spectral slope lies between  $-0.5$  and  $0.5$  (see Fig. 2).

### 3 NUMERICAL MODEL

Analytical model developed in Section 2.2 describes only the OIR synchrotron spectra and is valid for purely power-law electrons. Such distributions may result from various acceleration mechanisms such as shock acceleration or magnetic dissipation. In the limit of low optical depth and weak magnetic field the electrons are unable to cool and the shape of the distribution stays unchanged. These conditions might be satisfied in quiescent state, for which the analytical model can be applied. During the accretion outbursts the matter density in the hot flow increases and the energy exchange and cooling processes become important, thus the initial power-law distribution evolves. The most important mechanisms operating in the hot rarefied plasmas of the hot accretion flows are Compton scattering, synchrotron emission and absorption, Coulomb collisions, bremsstrahlung, and possibly photon-photon pair production and annihilation. At high energies, for a continuously operating acceleration, the steady state distribution remains a power-law-like, but softens because of cooling by Compton, synchrotron and bremsstrahlung. At lower energies, Coulomb collisions and synchrotron self-absorption efficiently thermalize particles, forming a Maxwellian distribution. The total particle distribution consists of a low-energy Maxwellian plus a high-energy tail. Such a distribution we call hybrid. The shape and energy content of the tail are fully determined by the balance between acceleration and cooling processes. It cannot be calculated analytically, therefore we treat this problem numerically. The photon spectrum emitted by the hot flow is computed self-consistently with the particle distributions.

The time-scale of equilibration of electron and photon distributions for typical parameters of our model is smaller than the corresponding advection time in the hot flow (see Appendix A). Thus we can use an assumption that the electron and photon distributions are in a steady-state. We obtain them by solving the relevant kinetic equations.

#### 3.1 Model set up

We represent the inner accretion flow with a number of separate regions (zones), embedded one into another (Fig. 1). Each zone  $i$  has size  $R_{i+1} - R_i$  of the order of its height  $H_i \sim (R_{i+1} + R_i)/2$ . We assume that the inner hot flow corresponds to some type of radiatively inefficient accretion flow (see review in Kato et al. 1998). In such flow, the radiative loss rate per unit area scales with

<sup>1</sup> Precise calculations of additional contribution from optically thin parts result in a slightly different normalization, while the spectral slope remains the same (see Marscher 1977).



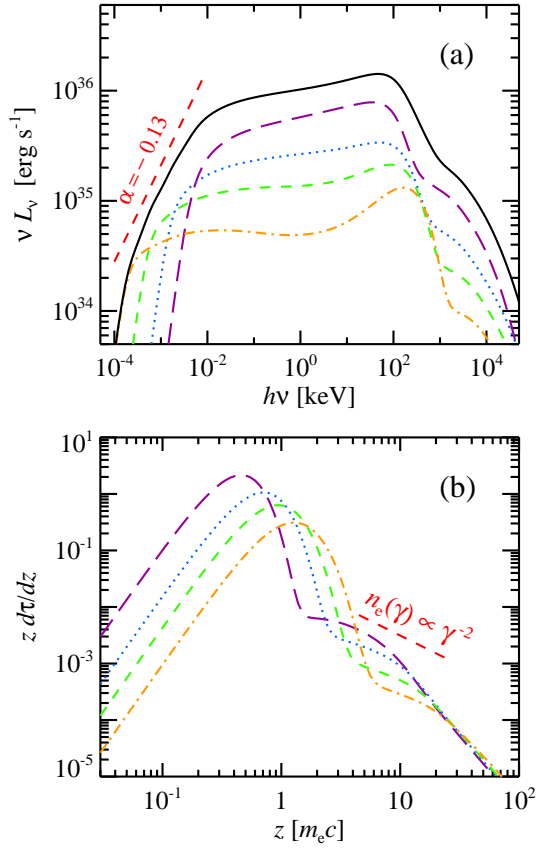


**Figure 3.** Photon spectra (upper panel) and electron distributions (lower panel) for the hard-state model with initial electron injection index  $\Gamma_{\text{inj}} = 2.5$ . Electron momenta  $z = \sqrt{\gamma^2 - 1}$  are measured in units of  $m_e c$ . Other parameters are listed in Table 1. The lines correspond to zone 1 (long-dashed), zone 2 (dotted), zone 3 (dashed) and zone 4 (dot-dashed). Sum of the components is shown with solid line. Red short-dashed line shows the slopes from analytical approximation. For further details, see Section 3.2.

radius as  $Q_{\text{rad}} \propto R^{-5/2}$ , and the electron density scales as  $\rho \propto R^{-3/2}$ , thus the overall scalings for the luminosity and Thomson optical depth of  $i$ -th zone are

$$L_i \propto \int_{R_i}^{R_{i+1}} Q_{\text{rad}}(R) R dR \propto \frac{1}{\sqrt{R_i}} - \frac{1}{\sqrt{R_{i+1}}}, \quad (8)$$

$$\tau_i \propto \int_{R_i}^{R_{i+1}} \rho(R) dR \propto \frac{1}{\sqrt{R_i}} - \frac{1}{\sqrt{R_{i+1}}}. \quad (9)$$

The scaling of the magnetic field with radius is model-dependent (e.g., Shadmehri & Khajenabi 2005; Meier 2005; Akizuki & Fukue 2006). Here we assume that the magnetic pressure and the radiation pressure are equal throughout the flow, from which we get  $B \propto R^{-5/4}$ . The latter scaling is the same as in the accretion flow model of Shadmehri & Khajenabi (2005).

The electron heating is simulated as a power-law injection with slope  $\Gamma_{\text{inj}}$ , extending between the Lorentz factors 1 and  $10^3$ . Net energy input in  $i$ -th zone equals to the luminosity  $L_i$ . This energy is redistributed between the particles (electrons and positrons) and photons in processes of synchrotron emission and self-absorption, Compton scattering, Coulomb collisions, pair production and annihilation and bremsstrahlung emission. The domi-

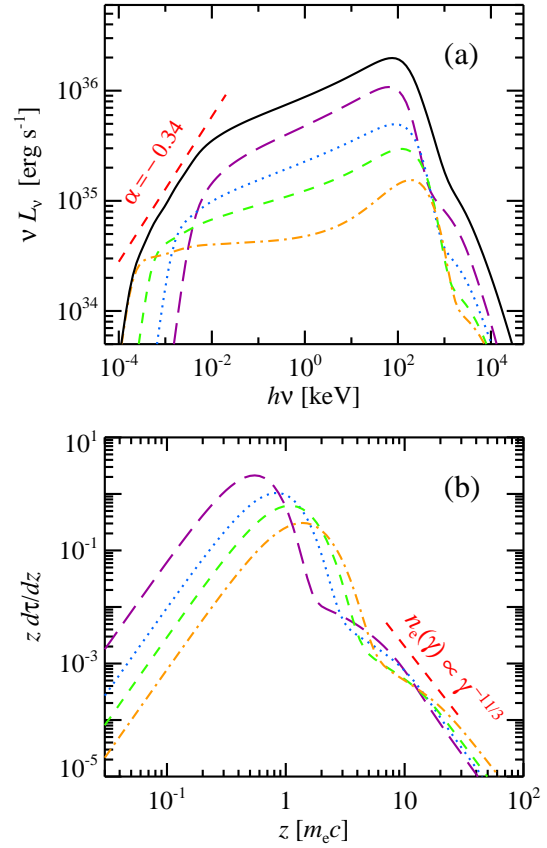


**Figure 4.** Same as Fig. 3, but for the electron injection index  $\Gamma_{\text{inj}} = 3.0$ . X-ray spectra are harder in this case, while the OIR spectrum is softer.

nating cooling regime for a specific electron Lorentz factor depends on the parameters of the region: size, magnetic field and optical depth (relevant scaling is given in Appendix A). In addition to the internally produced radiation, we also consider soft photons from the cold outer accretion disc in the form of the blackbody radiation injected homogeneously into the system. The parameters that describe them are the colour temperature  $T_{\text{col}}$  and the ratio of the disc to the  $i$ -th zone luminosity  $f = \Omega_i L_{\text{disc}}/L_i$ . Here the factor  $\Omega_i$  accounts for the fact that only a part of the disc luminosity is entering the hot flow. It is fully determined by the cold disc/hot flow geometry and in our case is

$$\Omega_i \approx \frac{1}{4} \left( \frac{R_i}{R_{\text{d,in}}} \right)^3, \quad (10)$$

where  $R_{\text{d,in}}$  is the disc truncation radius,  $(R_i/R_{\text{d,in}})^2/4$  is the dilution factor of the  $i$ -th zone, as seen from the cold accretion disc, and another factor of  $R_i/R_{\text{d,in}}$  accounts for anisotropy of the disc radiation. Photon escape from each zone, giving rise to the observed emission, is modelled in terms of escape time. The kinetic equations for electrons and photons describing these processes are solved using the code described in Vurm & Poutanen (2009). The total spectrum of the flow is the sum of spectra from each zone. The spectrum of  $i$ -th zone is computed under the approximation of homogeneous isotropic distributions in a sphere of radius  $R_{i+1}$ .

The model has seven parameters (i) the total luminosity, (ii) the index of the electron power-law tail (constant throughout the flow), (iii) the electron Thomson optical depth and (iv) the mag-

**Table 1.** Parameters of the multi-zone hot inner flow model.

Parameter / zone	1	2	3	4
$R_i/R_S$	3	10	30	100
$R_{i+1}/R_S$	10	30	100	300
$\tau$	2.5	1.3	0.8	0.4
$B$ ( $10^6$ G)	1	0.25	0.06	0.015
$L_i$ ( $10^{36}$ erg s $^{-1}$ )	6	3	2	1
$kT_{\text{col}}^a$ (keV)	–	0.25	0.12	0.05

<sup>a</sup>  $kT_{\text{col}}$  is the colour temperature of radiation coming into the hot flow from the inner edge of the cold accretion disc extended up to  $R_{i+1}$ .

netic field in the innermost regions, (v-vi) indices of their power-law radial dependencies  $\theta$  and  $\beta$ , and (vii) the hot flow size.

### 3.2 Hard state

In the hard state, the hot flow extends to large radii  $\gtrsim 100R_S$  and the role of the soft photons from outer cold accretion disc is negligible. Therefore, we neglect them in the simulations and consider only the emission from the hot flow. We take the total luminosity of the flow of  $L = 10^{-2} L_{\text{Edd}}$  ( $L_{\text{Edd}}$  is the Eddington luminosity), the Thomson optical depth of the innermost zone  $i = 1$  of  $\tau = 2.5$ , typically found from the X-ray/ $\gamma$ -ray data (e.g. Zdziarski et al. 1998; Frontera et al. 2001b), and magnetic field  $B = 10^6$  G. The radial dependencies of the parameters are given in Sect. 3.1 and listed for each zone in Table 1 (first five rows). The results of simulations are shown in Fig. 3 for the injection slope  $\Gamma_{\text{inj}} = 2.5$  and in Fig. 4 for  $\Gamma_{\text{inj}} = 3.0$ .

Simulations show, that larger zones generally have softer spectra. The main reason is that the outer zones are more transparent to the synchrotron radiation, which increases the ratio of the synchrotron to the thermal Compton luminosities. At the same time we see that the equilibrium electron temperature grows with radius from approximately 40 keV up to 180 keV. This is caused by a significant drop of the optical depth  $\tau$  in the outer zones, with a relatively slow change of the Compton  $y$ -parameter. The X-ray spectrum of the outer zones is dominated by thermal bremsstrahlung, because its role relative to Compton cooling  $\propto \tau R/L$  grows linearly with radius (eq. (22) in Veledina et al. 2011b). The combined spectrum of all zones has a concave shape, exactly as observed (Ibragimov et al. 2005).

The high-energy tail above a few 100 keV is dominated by Comptonization produced by the non-thermal electron tail. At Lorentz factor above 20, the tail has a power-law shape corresponding to index  $p = \Gamma_{\text{inj}} + 1$  due to synchrotron and Compton cooling. At intermediate  $\gamma$ , the distribution is curved, because of the large role of Coulomb collisions which produce equilibrium distribution with index  $p = \Gamma_{\text{inj}} - 1$  (eq. (12) in Veledina et al. 2011b).

The OIR spectrum is produced by a combination of synchrotron self-absorption peaks from different zones. The outer zones dominate at lower frequencies. The low-energy cut-off is determined by the size of the largest zone, which for  $R = 300R_S$  is at 0.2 eV. At even lower energies, the spectrum is  $L_\nu \propto \nu^{5/2}$ . Above 10 eV, emission from all zones is optically thin and is dominated by thermal Comptonization of seed non-thermal synchrotron photons.

The X-ray spectra are harder for  $\Gamma_{\text{inj}} = 3.0$ . This is a direct consequence of the softer equilibrium electron distribution, which results in a lower synchrotron luminosity and larger Comp-

ton  $y$ -parameter. The OIR spectra are, however, softer in this case, because a different slope of the electron non-thermal tail results in a relatively low normalization of the electron distribution and, respectively, in the weaker synchrotron emission from the inner zones.

Many of the numerical results can be understood from the analytical model if one approximates the electron distribution by a power-law in the energy range, where electrons emit close to the self-absorption frequency. For our simulations these electrons have Lorentz factors  $\gamma_t \approx 10$ .

In the case of injection slope  $\Gamma_{\text{inj}} = 2.5$  the optical depth of the power-law electrons scales the same way as the total optical depth, with index  $\theta = 1/2$  (see Fig. 3b). The slope of the electron distribution is approximately  $p = 2$ . Putting these parameters (with  $\beta = 5/4$ ) into equation (7), we get  $\alpha_{\text{OIR}} = -0.13$ , in good agreement with the numerically computed slope (see Fig. 3a).

For softer electron injection  $\Gamma_{\text{inj}} = 3.0$ , we find that the optical depth at the Lorentz factor  $\gamma_t = 10$  is nearly constant for every zone (see Fig. 4b), thus for analytical approximation we take  $\theta = 0$ . The average electron slope at this Lorentz factor is  $p \approx 11/3$ . Putting these coefficients into equation (7), we get  $\alpha = -0.34$ , also in good agreement with the computed spectrum (Fig. 4a).

The turnover of the synchrotron spectrum from each radius is given by equations (3) and (4). For the case with  $\Gamma_{\text{inj}} = 2.5$  we substitute parameters of zone 1:  $R = 10R_S$ ,  $B = 10^6$  G,  $\tau = 10^{-2}$  (Thomson optical depth of the high-energy tail), and power-law slopes  $\beta = 5/4$ ,  $\theta = 1/2$  and  $p = 2$  we obtain the scaling

$$\nu_t \approx 10^{15} \left( \frac{R}{10R_S} \right)^{-1} \text{ Hz.} \quad (11)$$

The similar scaling can be obtained for  $\Gamma_{\text{inj}} = 3.0$ . In order to estimate the synchrotron luminosity we substitute the calculated turn-over frequency into equation (6)

$$\nu L_\nu \approx 2 \times 10^{35} \left( \frac{R}{10R_S} \right)^{-7/8} \text{ erg s}^{-1}, \quad (12)$$

which is consistent (within a factor of two) with the values obtained in precise numerical calculations.

As we mentioned above, the precise values of the minimum and maximum Lorentz factors of the power-law electrons do not affect much the resulting spectra. The main model parameters (see Sect. 3.1) can be constrained by the data. The first four parameters can be obtained from the X-ray luminosity and spectral slope, the cut-off temperature and the slope of the  $\gamma$ -ray tail. The final three parameters can then be extracted from the OIR data: the turn-over frequency (equation 3), spectral slope (equation 7) and the luminosity (equation 6).

### 3.3 State transitions

A generally accepted scenario for the hard to soft state transition involves the motion of the cold accretion disc towards the compact object (Poutanen et al. 1997; Esin et al. 1997, 1998). In this case, the role of the disc increases and it gradually replaces the synchrotron as a source of seed photons for Comptonization. We simulate this action by replacing the spectrum in the corresponding zone of the hot flow with a multi-colour blackbody disc (Shakura & Sunyaev 1973; Frank et al. 2002) of an appropriate inner radius. We take the disc truncation radius  $R_{\text{d,in}}$  equal to the outer radius of the largest zone of the hot flow and we keep the outer disc radius at  $R_{\text{d,out}} = 3 \times 10^4 R_S$ .

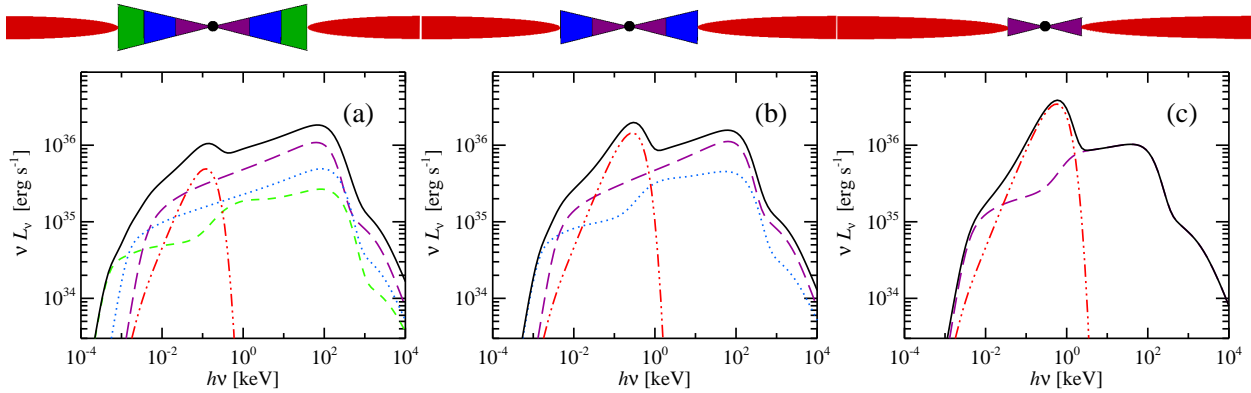


**Figure 5.** *Upper panels:* geometrical evolution at state transition. Principal components are standard accretion disc (red) and inner hot flow: zone 1 (within  $10R_S$ , violet), zone 2 (within  $30R_S$ , blue) and zone 3 (within  $100R_S$ , green). *Lower panels:* spectral evolution at state transition. Contribution of different zones are marked with lines: zone 1 (long-dashed), zone 2 (dotted), zone 3 (short-dashed) and thin accretion disc (three-dot-dashed). Colour coding is the same as in the upper panels. The inner radius of the truncated accretion disc changes from (a)  $100R_S$  through (b)  $30R_S$  to (c)  $10R_S$ , replacing the corresponding zones of the hot flow.

The additional seed photons for Comptonization are modelled by the injection of blackbody photons with temperature corresponding to the colour temperature of disc inner radius:

$$kT_{\text{col}} = 2.3 \left( \frac{L}{L_{\text{Edd}}} \right)^{1/4} \left( \frac{3R_S}{R_{\text{d,in}}} \right)^{3/4} \left( 1 - \sqrt{\frac{3R_S}{R_{\text{d,in}}}} \right)^{1/4} \text{ keV} \quad (13)$$

(see Table 1). Given that the transition occurs at almost constant luminosity (see Done et al. 2007), we assume the luminosity, magnetic field and Thomson optical depth of each hot flow zone remain the same as in the hard state (see Table 1). The relative contribution of the cold disc and the hot flow in the observed spectrum depend on the inclination, which we take equal to 60 degrees. The resulting spectra are shown in Fig. 5.

The total spectrum is now composed of synchrotron and bremsstrahlung photons, as well as Comptonized synchrotron and disc radiation. The transition between the later two emission spectra is reflected in the overall spectral curvature at  $\sim 0.1$  keV in the spectra of the largest hot-flow zone (see Fig. 5). In this zone the disc is the dominant source of seed photons. The cool disc luminosity grows when it moves towards the black hole and its photons are much more energetic than those provided by the synchrotron mechanism, thus the X-ray spectrum softens as the transition proceeds. At the same time, the outer regions of the hot flow collapse, leading to a dramatic drop in luminosity at  $\sim 0.1$  eV. The (low) cut-off frequency increases and the OIR spectrum becomes harder (see Fig. 6). Relatively small changes occur around  $E \sim 10$  eV. Fig. 6(b) shows the  $L_\nu$  spectra in more details. Here we see that the pure hot-flow spectrum below the cut-off in the IR band is a power-law with index  $\alpha = 5/2$  corresponding to the optically thick non-thermal synchrotron. Once the truncation radius decreases to  $10R_S$ , the spectrum becomes a combination of the disc and non-thermal synchrotron, resulting in a softer spectrum with  $\alpha \approx 2$ .<sup>2</sup>

Hence, one would expect fast change in the luminosity at OIR wavelengths, while (almost) no change in the UV. For instance, if one observes the collapse of the  $100R_S$  zone while the  $30R_S$  zone is still present, there will be huge changes at  $\sim 0.5$  eV, while not

so significant changes at  $\sim 2$  eV. The opposite is expected during the soft-to-hard state transition: when the disc recedes, the hot flow occupies larger and larger radii and its synchrotron luminosity increases earlier at shorter wavelengths.

Fig. 7 illustrates possible spectral features appearing for different sizes of the outer disc radius. We see that the hot flow completely dominates the spectrum below  $\sim 10$  eV if its size is larger than  $100R_S$ . In this case, the exact value of  $R_{\text{d,out}}$  does not play any role (unless reprocessing in the outer disc starts to be important). The largest changes occur for smaller truncation radius and large  $R_{\text{d,out}} = 10^6 R_S$ . For such large discs (see Fig. 7(a)), radiation in the far IR is dominated by the Rayleigh-Jeans part of the spectrum from the outer cold disc. The UV radiation is mostly produced at the inner disc edge. Synchrotron from the hot flow is still important in the optical.

#### 4 COMPARISON WITH OBSERVATIONS

In the present work we considered an inhomogeneous hot accretion flow model for the broadband spectra of the accreting black holes. In the hard state, when the standard cold disc is truncated at a large radius, the central hot region is radiating mostly via thermal Comptonization of the non-thermal synchrotron photons. Hot flow extending over a large range of radii produces a power-law-like flat spectrum in the OIR range.

In the soft state, the cold disc moves in, brightens and takes over as a source of seed soft photons for Comptonization. This effectively reduces the role of synchrotron radiation in electron cooling. At the same time, the reduction of the size of the emitting region results in an increase of the synchrotron self-absorption frequency, making the synchrotron emission in the IR band negligible.

The scenario considered in this work is capable of reproducing the broadband spectra from the IR to the gamma-rays of black holes in all spectral states. However, the spectral data alone are not capable of distinguishing among various models and they have to be considered together with other sources of information (e.g. timing and polarization). Below we will discuss in details various properties of the developed hot flow model and compare them to observations. We also compare our model to the popular jet scenario.

<sup>2</sup> Further softening of the spectrum is expected if the cold disc penetrates into the hot flow forming a corona-like geometry. This results in additional cooling by the disc photons and reduction of the Compton  $y$ -parameter.

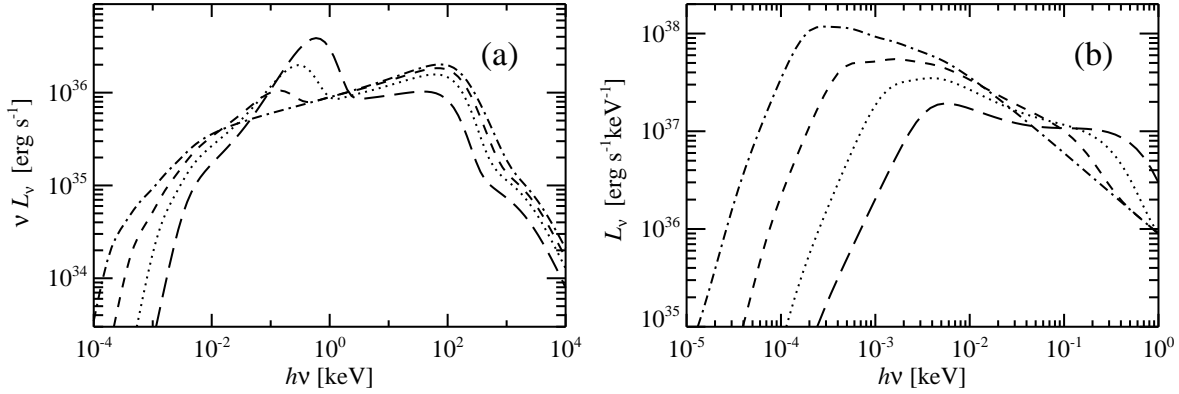


**Figure 6.** Spectral evolution at state transition: the pure hot-flow spectrum (dot-dashed lines), and spectra of the hot flow with the cold disc truncated at  $100R_S$  (short-dashed),  $30R_S$  (dotted), and  $10R_S$  (long-dashed). (a) spectra in  $\nu L_\nu$  units and (b) spectra in  $L_\nu$  units (note the different photon energy range). Here the outer disc radius is  $R_{d,out} = 3 \times 10^4 R_S$ .

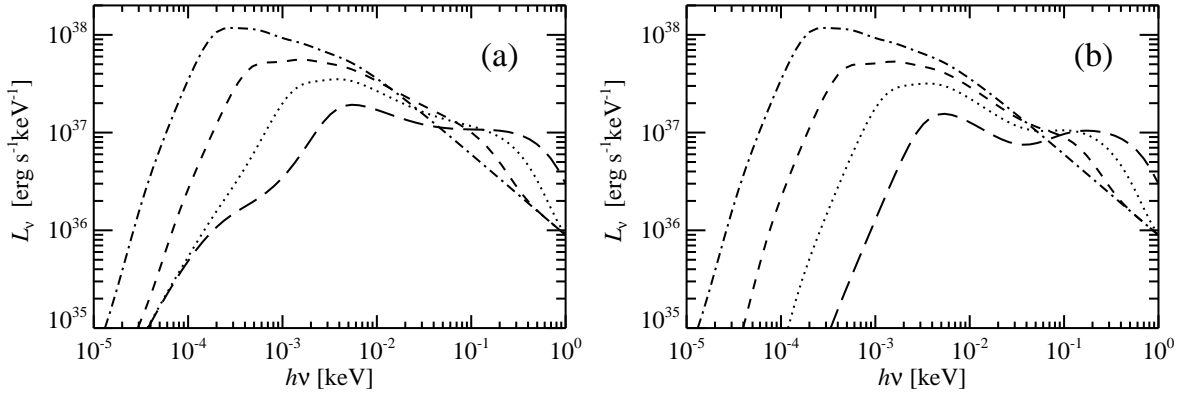


**Figure 7.** Same as in Fig. 6b, but for outer disc radii (a)  $R_{d,out} = 10^6 R_S$  and (b)  $R_{d,out} = 300 R_S$ .

## 4.1 Hard state

### 4.1.1 X-ray spectrum and variability

In our model the X-ray spectrum is dominated by the Comptonization continuum from the innermost zone where most of the gravitational energy is dissipated. In the X-ray range it can generally be described by a power-law. Outer zones of the hot flow have softer spectra, because of a larger role of non-thermal synchrotron and the increasing amount of the cold disc photons. The overall spectrum is thus slightly concave. Such spectra are consistent with those observed from the black holes. For example, the best studied black hole, Cyg X-1, clearly has a concave spectrum (Frontera et al. 2001a) that can be fitted with two Comptonization continua (Ibragimov et al. 2005).

A larger contribution from the outer zones to the soft X-rays should be reflected in the variability properties. Assuming that variability is produced by propagation of fluctuations in the mass accretion rate through the disc (Lyubarskii 1997; Kotov et al. 2001), we expect an increase in the variability amplitude for higher photon energies at higher Fourier frequencies, which is indeed observed (Nowak et al. 1999a). The autocorrelation function of soft X-rays in our model is expected to be wider than that of the hard X-rays, consistent with what is measured in Cyg X-1 (Maccarone et al. 2000). The same effect is more obviously seen in the Fourier-frequency-resolved spectra (Revnivtsev et al. 1999; Gilfanov et al.

2000), which are softer and have larger reflection amplitude at low Fourier frequencies. This implies that soft X-rays are mostly produced in the outer zones of the hot flow, closer to the cold reflecting medium. The reduction of the equivalent width of the 6.4 keV Fe line in the frequency-resolved spectra above 1 Hz suggests that the cold disc truncation radius is of the order of 100 Schwarzschild radii (Revnivtsev et al. 1999; Gilfanov et al. 2000), further supporting our scenario. Similarly, even larger inner radii of the cold disc were measured in the low-extinction black hole transient XTE J1118+480 (Esin et al. 2001; Chaty et al. 2003).

Another important finding is that the harder X-rays are delayed with respect to the soft X-rays (Nowak et al. 1999a,b). The large values of these hard time lags and their frequency-dependence  $f^{-1}$  can naturally be explained by spectral pivoting of a power-law-like spectrum (Poutanen & Fabian 1999; Poutanen 2001). The spectral evolution can arise when the accretion rate fluctuations propagate towards the black hole into the zone with harder spectra (Kotov et al. 2001), again consistent with our multi-zone hot flow model.

### 4.1.2 OIR excesses and flat spectra

The OIR excesses above the standard disc spectrum were reported in a number of sources: XTE J1859+226 (Hynes et al. 2002), XTE J1118+480 (Hannikainen et al. 2000; Esin et al.



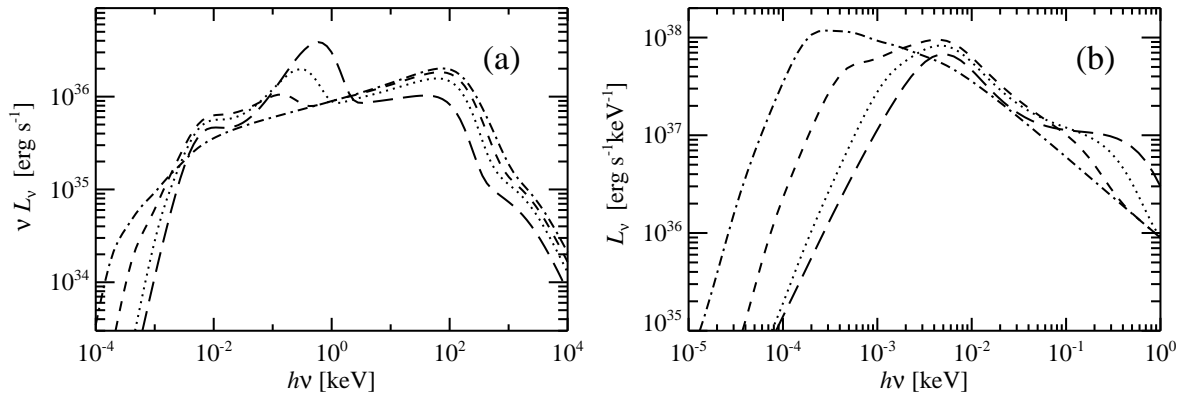


**Figure 8.** Same as in Fig. 6, but with the additional contribution from the irradiated accretion disc.

2001; Chaty et al. 2003), GX 339–4 (e.g., Gandhi et al. 2011; Shidatsu et al. 2011), A0620–00 (Gallo et al. 2007), SWIFT J1753.5–0127 (Chiang et al. 2010), V404 Cyg (Hynes et al. 2009a). In our model, the OIR spectrum consists of two components (Fig. 5): one comes from the multi-colour accretion disc and another from the hot flow. The relative role of these components varies with the wavelength (Figs 6 and 7). The disc spectrum is hard in the OIR band, while the non-thermal synchrotron from the hot flow is typically softer with  $\alpha_{\text{OIR}} \sim 0$ . The second component thus produces an excess emission.

In many cases the contribution of the non-thermal component is rather small compared to the disc, and it can be seen only as the IR excess. On the other hand, sometimes the synchrotron component dominates, which results in an almost pure power-law OIR spectrum. A good example is XTE J1118+480, where the spectral index  $\alpha_{\text{OIR}} = -0.15$  was measured (Chaty et al. 2003). This spectral index can be reproduced in our model, for example, with parameters  $\theta = 0.5$ ,  $p = 2.0$  and  $\beta = 5/4$  (Fig. 3 illustrates this case).

#### 4.1.3 Optical/X-ray cross-correlation

In recent years, a number of simultaneous optical(IR,UV)/X-ray observations with high time resolution were performed (Kanbach et al. 2001; Hynes et al. 2003; Gandhi et al. 2008; Hynes et al. 2009b; Durant et al. 2011), all revealing the intrinsic connection of the two light curves on subsecond time-scales. The computed cross-correlation functions have complicated shape with a dip in the optical light curve preceding the X-ray peak (the so-called precognition dip), together with an optical peak lagging the X-rays.

The behaviour can be explained if the optical emission consists of two components: one coming from the synchrotron in the hot flow and another from reprocessed X-ray emission (Veledina et al. 2011a). Increase of the mass accretion rate causes an increase in the X-ray luminosity and affects the parameters of the hot flow, leading to a higher synchrotron self-absorption. The latter results in a drop of the optical emission, therefore these two energy bands appear anticorrelated. This is reflected in the negative CCF with the shape resembling that of the X-ray auto-correlation function. On the other hand, the reprocessed radiation is delayed and smeared, giving rise to a less sharp CCF peaking at positive lags (optical delay). The combined CCF has a complicated shape consistent with the data. From the point of view of the multi-zone

consideration, with small increase of mass accretion rate the cool disc moves inwards and causes the collapse of the hot flow at large radii. Thus the suppression of the OIR emission with increasing X-ray radiation is also expected in this scenario.

A different, one-peak structure of the IR/X-ray cross-correlation function was found in GX 339–4 (Casella et al. 2010), suggesting the hot flow was not the dominant source of the correlated variability during their observations. However, it might still give significant contribution to the constant flux component, but less to the varying component, and therefore would not be detected in the timing analysis. As it can be seen from Figs 3 and 4, the zones giving major contribution to the IR wavelengths do not contribute much to the X-rays. Therefore, the fraction of the correlated variability coming from these regions is expected to be small, and another source (likely the jet emission, as suggested in Casella et al. 2010) is responsible for the shape of the cross-correlation function.

The optical correlation with the X-rays was also detected in the quiescent state of V404 Cyg (Hynes et al. 2009a), while no clear radio/X-ray (nor radio/optical) correlation was found on the time-scales of hours, again suggesting the radio and optical emission are not produced by the same component.

#### 4.1.4 Irradiation of the cold disc

The X-ray radiation from the hot flow can be intercepted and reprocessed in the cold disc. The irradiation strongly depends on the disc outer radius and the disc shape. The larger is  $R_{\text{d,out}}$ , the cooler can be this emission. The more flared is the disc, the larger is the reprocessed luminosity, which typically is expected to give significant contribution to the OIR band, exceeding the viscous disc luminosity at these energies (Shakura & Sunyaev 1973). Presence of the irradiated disc can be also reflected in the X-ray time-lags (see Poutanen 2002, and reference therein) and in the optical/X-ray cross-correlation function (Veledina et al. 2011a). It is also seen in the spectrum (e.g., Hynes et al. 2002; Gierliński et al. 2009).

For typical parameters of LMXBs with the disc size of  $10^{11}$  cm, the X-ray luminosity of  $10^{37}$  erg s $^{-1}$  and 10 per cent reprocessing efficiency, the temperature of the outer disc is about 1.2 eV. For an illustration, we have added the emission from the irradiated discs to our hot-flow spectra (see Fig. 8). Following Cunningham (1976), we assumed the following dependence of the effective temperature on radius

$$kT_{\text{irr}} = 1.2 \left( \frac{R}{R_{\text{d,out}}} \right)^{-3/7} \text{ eV} \quad (14)$$

and the outer disc radius of  $R_{\text{d,out}} = 10^{11}$  cm.

As can be seen in Fig. 8, for typical parameters of the BHBs the spectrum of the irradiated disc peaks around 5 eV and has a Rayleigh-Jeans-like tail with  $\alpha \sim 2$  in the OIR. If the inner hot flow size exceeds 30–100  $R_{\text{S}}$ , its synchrotron emission will dominate over the reprocessing below  $\sim 1$  eV. We do not expect much of reprocessed emission below 0.5 eV, except for the large-period systems (similar to V404 Cyg and GRS 1915+105). Therefore, at sufficiently long wavelengths we expect the IR/X-ray cross-correlation function to have only the dip, with no peak. The overall spectral shape is complex, with a number of bumps corresponding to the standard disc (above  $\sim 100$  eV), the irradiated disc and synchrotron from the hot flow (in the 1–10 eV range). A hardening of the spectrum observed in GX 339–4 at  $\sim 2$ –3 eV (Buxton et al. 2012; Dincer et al. 2012; Rahoui et al. 2012) can be due to a transition from the hot-flow to the irradiated disc spectrum.

## 4.2 State transition

### 4.2.1 Broadband spectral evolution at state transition

During the hard-to-soft state transition the outer zones of the hot flow gradually collapse. This leads to a drop in luminosity at longer wavelengths preceding the subsequent drop at shorter wavelengths. Such behaviour was found in the UV data of the GX 339–4 during the 2010 outburst (Yan & Yu 2012). The opposite is expected at the reverse transition, namely, the fast luminosity increase occurs earlier at shorter wavelengths.

Recently, the entire transition of the BH transient XTE J1550–564 from hard to the soft state and back was monitored in the V, I and H filters (Russell et al. 2011). Just before the X-ray spectral transition as well as after the reverse transition, significant colour variations occurred, as indicated by the rapid changes in the H band at almost constant V magnitude.

In terms of our model, the observed colour change is related to the collapse/recover of a zone in the hot flow that is responsible for the H-band emission (see Section 3.3). As is known, the hard-soft and the soft-hard spectral transitions occur at different X-ray luminosities (e.g. Zdziarski et al. 2004). This hysteresis most probably is related to the fact that at the same luminosity the cold disc is further away from the central source on the rising phase of the outburst, than on the decline. According to our model, the hysteresis has to be reflected also in the OIR spectra, namely the fast colour change should occur at a higher X-ray luminosity on the rising phase, than on the decline. This is indeed observed (Russell et al. 2011).

In the soft state, the accretion disc extends to the last stable orbit, leaving no possibility for the inner hot flow to exist. However, the corona should still be present as supported by the existence of the non-thermal tails (produced by the inverse Compton scattering of the disc photons). It may also produce synchrotron radiation in the OIR band, but likely at a lower level.

### 4.2.2 Change of the X-ray radiation mechanism

At luminosities above a few per cent of Eddington, there is a strong correlation between spectral index and luminosity. At lower luminosities the trend is reversed (Sobolewska et al. 2011). Similarly, an indication of the reverse trend was detected in low-luminosity AGNs (Constantin et al. 2009). This was interpreted as a change of the source of seed photons for Comptonization from the disc photons dominating at higher luminosities to the synchrotron at lower

luminosities. The anti-correlation at  $L/L_{\text{Edd}} \sim 10^{-3}$ – $10^{-2}$  can be reproduced within a two-temperature hot accretion flow model (Niedźwiecki et al. 2012). The whole spectral index – luminosity dependence is well explained by one-zone hybrid Comptonization model (see figs 7 and 12 in Veledina et al. 2011b). The multi-zone consideration presented in the current paper follows the same pattern as the one-zone model, because the X-ray spectrum is dominated by radiation from the inner zone.

## 4.3 Polarization

The only indication of the X-ray polarization from BHB goes back to the OSO-8 satellite (Weisskopf et al. 1977), which measured  $3.1 \pm 1.7$  per cent linear polarization from Cyg X-1 at 2.6 keV. Such a polarization can be produced by Compton scattering if the geometry of the X-ray emitting region is a flattened disc-like structure ( $H/R \sim 0.2$  according to the calculations of Lightman & Shapiro 1976). The number of scatterings the X-ray photons undergo depends on the electron and the seed photon temperatures. For a 100 keV plasma, photons double their energy in each scattering, hence the disc photons of a typical energy of 0.5 keV would reach 3 keV in only 3 scatterings, while the synchrotron photons emitted at 10 eV require about 8 scatterings. Thus even if the synchrotron photons are polarized, this information is forgotten, and the X-ray polarization is completely determined by the geometry of the medium. In our model, we considered the simplest case of  $H \sim R$ , however, the spectral shape remains the same even for the flatter geometry, thus the polarization measurements are consistent with the hot flow model.

The polarization degree of the hot flow radiation in the OIR band strongly depends on the magnetic field structure. Synchrotron emission from non-thermal electrons can have a large polarization degree (up to 70 per cent) in the optically thin part of the spectrum. A high polarization in radio and optical reaching 30–50 per cent is indeed observed from extragalactic relativistic jets (Impey et al. 1991; Wills et al. 1992; Lister 2001; Marscher et al. 2002; Ikejiri et al. 2011). In the optically thick regime, polarization is about 10 per cent and has a different sign (Pacholczyk & Swihart 1967; Ginzburg & Syrovatskii 1969). In the hot flow model, the synchrotron OIR power-law spectra are produced by combination of self-absorption peaks from different hot flow radii, therefore, even for a highly ordered magnetic field the polarization unlikely reaches the theoretical limits. For a less ordered magnetic field, expected in a turbulent medium, the polarization levels of synchrotron radiation are expected to be very low.

Optical and UV radiation from the accretion disc may also be polarized up to  $\sim 11.7$  per cent (parallel to the disc plane) at large inclinations, if the opacity is dominated by the electron scattering (Chandrasekhar 1960; Sobolev 1963). At lower energies, absorption in the atmospheric layers of the disc reduces the polarization degree (Loskutov & Sobolev 1981, 1982) and it can drop down to zero in the IR. A detection of linear polarization at a few per cent level in the OIR bands in BHBs (Schultz et al. 2004; Shahbaz et al. 2008; Russell & Fender 2008; Chaty et al. 2011) is thus more consistent with being produced by synchrotron radiation with rather tangled magnetic field, and can originate either from the hot flow or from the jet. In the next section we make a detailed comparison between these two sources.

#### 4.4 Comparison with the jet paradigm

The simplest jet model has a conical geometry with all parameters distributed as a power-law with distance and with electrons having a power-law distribution in Lorentz factor (Marscher 1977; Blandford & Königl 1979). The magnetic field can be assumed ordered or tangled, but this only influences the polarization properties. The mathematical formulation of this model is identical to the analytical model for the hot flow considered in Sect. 2. Such simplified jet model was applied to the broadband spectra of BHBs (Markoff et al. 2001). In a more realistic situation, the electron distribution would be subject to acceleration mechanisms, as well as cooling processes such as Compton, synchrotron and adiabatic (as e.g. in Pe'er & Casella 2009; Pe'er & Markoff 2012). However, due to a complicated physics, the energy input and the acceleration efficiency throughout the jet are generally unknown, and in the spectral models remain ad hoc functions. This disadvantage is avoided in the hot flow models, as the input energy comes from the liberated gravitational energy, which can be estimated analytically. Both models, however, suffer from a large number of parameters and from an unspecified acceleration mechanism.

Apart from the different physical assumptions, the jet and the hot flow models predict different spectral properties. In the simple jet model, the synchrotron spectrum consists of the optically thin part with spectral slope  $\alpha = -(p - 1)/2$  and the optically thick part (sum of contribution from different zones) with the same slope as given by equation (7). The low-energy cut-off is determined by the jet extension and falls in the radio wavelengths. In contrast, the cut-off of the hot-flow spectrum is related to the truncation radius of the disc and likely falls in the OIR band. The break energy to the optically thin part of the jet is determined by the extension of the injection zone and typically is in the IR regime, while in the hot flow model it is in the UV band as determined by the size of the inner region. The jet optically thin synchrotron is claimed to extend to the X-rays, while in the hot flow model these energies are produced in Comptonization processes.

Let us now assess possible contribution of the jet and the hot flow to various wavelengths relying on the observed spectral properties. The X-ray spectra of BHBs have sharp cutoffs at about 100 keV that are impossible to produce by non-thermal synchrotron even if the electron distribution has an abrupt cutoff (Zdziarski et al. 2003). The hard spectra are also difficult to produce by optically thin synchrotron as this requires a very hard injection. Another question is then the observed low level of the X-ray polarization, which is in contradiction to the theoretical expectations from the optically thin synchrotron, as well as to the levels measured in extragalactic sources. On the other hand, the X-ray spectral properties are well explained by the (nearly) thermal Comptonization in the hot flow (see Sect. 4.1.1).

Atop of the X-ray power-law, the Compton reflection and the iron line are rather often detected features. Their amplitude and its correlation with the underlying spectral shape strongly argue in favour of the small X-ray emission region and against any beamed-away radiation from the jet. The analysis of the hard state X-ray spectra of the BHB Cyg X-1 revealed that the spectra pivot at energies of 10–50 keV (Zdziarski et al. 2002). If the entire IR-to-X-ray continuum is produced by the same region (as proposed in the jet model), such pivoting would predict two orders of magnitude variations at 1 eV in the hard state, which are not observed. On the contrary, X-ray pivoting can be easily understood in the hot flow model, where it can be produced by small variations of the cold disc radius and varying injection rate of the disc photons (see Fig. 8).

The observed fast X-ray variability and hard time lags can naturally be understood in the hot flow model, where the X-ray emitting region is small, and the lags are related to the viscous time-scale of propagating fluctuations. At the same time, the lags can occur from Compton scattering delays within the jet (Kylafis et al. 2008), however, this model contradicts the observed narrowing of the auto-correlation function with energy (Maccarone et al. 2000).

The MeV tails detected in spectra of a number of hard-state BHBs are likely produced by the non-thermal electrons, either by the optically thin synchrotron emission (as in the jet) or by the inverse Compton scattering (as in the hot flow). The detailed investigation of this tail showed that it can be explained by the high-energy end of the jet synchrotron emission, however in this case one needs to assume a very hard index of the electron power-law distribution  $p = 1.3 - 1.6$ , which is in conflict with standard acceleration models and observations (see Zdziarski et al. 2012, and references therein). At the same time, the hot flow SSC easily accounts for the MeV tails in the hard state as well as in the soft-state, when the jet is quenched.

The OIR radiation has often been interpreted as a jet emission (see review by Russell & Fender 2009). The similarities in the IR and radio light-curves in microquasars, such as GRS 1915+105 (Fender et al. 1997), indeed favour common source of variability. However, this scenario meets substantial problems in a number of other sources. For instance, in some systems the jet broken power-law model, normalized to fit the radio fluxes, significantly underpredicts the optical luminosity (Soleri et al. 2010; Cadolle Bel et al. 2011). Sometimes the OIR slope is different from the radio as, for example, in XTE J1118+480 the OIR spectrum with  $\alpha_{\text{OIR}} = -0.15$  is much softer than the radio spectrum with  $\alpha_{\text{R}} = 0.5$  (Chaty et al. 2003), but much harder than expected from the optically thin jet emission. A rather low values of the OIR polarization (at most a few per cent) observed in BHBs is clearly much below the high polarization observed in the extragalactic jets. This again argues against strong contribution of the optically thin jet to the total spectrum. The hot flow scenario can reproduce the observed flat OIR spectra, at the same time the slopes in the OIR and radio do not necessarily match, as they are produced in different regions (inflow and outflow).

The two models make different predictions for changes of the OIR spectrum during the state transitions. In the hot-flow scenario, the spectrum gradually hardens at hard-to-soft transition on the time-scales of days to weeks, corresponding to the typical time-scales on which the cold accretion disc evolves. It softens again at the reverse transition. On the other hand, one would not expect systematic changes of the jet spectral slope, as any fluctuations would propagate through the jet on time-scales of hours, much shorter than the state transition. Thus, it is expected to fade/recover with constant spectral shape.

In reality, the OIR can contain contributions from a number of components: the hot flow, the jet, and the cold accretion disc (likely irradiated). It is also possible that there is a dip in the microwave band, where the transition from the radio jet to the hot flow occurs. The dip can be detected in the far infrared/submillimeter wavelengths, which were not well covered in the past. It is thus of high interest to observe at these wavelengths, especially with the available capabilities of ALMA.



## 5 SUMMARY

The observed OIR flat spectra and the MeV tails evidence the significant role of non-thermal electrons in spectral formation of accreting black hole binaries. On the other hand, the commonly detected X-ray spectral cut-offs at  $\sim 100$  keV can be produced only by thermal particles. Whether these two populations belong to one component or originate from completely different places is debated. We present a model, where the entire infrared to X-ray/ $\gamma$ -ray continuum is produced by one component, the inhomogeneous hot accretion flow, present in the vicinity of compact object. The difference from the earlier studied hot geometrically thick optically thin flows is that the steady-state electron distribution in our model is hybrid, i.e. Maxwellian with a weak high-energy tail.

The X-ray spectra in our model are dominated by the radiation of the innermost regions of the hot flow. For this reason, the model inherits the advantages of the one-zone synchrotron self-Compton model (Poutanen & Vurm 2009; Malzac & Belmont 2009) that explains well the X-ray spectral properties of BHB in their hard state, such as

- (i) stable spectra with photon index  $\Gamma \sim 1.6$ – $1.9$  and the cutoff at  $\sim 100$  keV in the hard state,
- (ii) low level of the X-ray polarization,
- (iii) presence of the MeV tail in the hard state,
- (iv) power-law like X-ray spectra extending to a few MeV in the soft state,
- (v) softening of the X-ray spectrum with decreasing luminosity below  $\sim 10^{-2} L_{\text{Edd}}$ ,
- (vi) weakness of the cold accretion disc component in the hard state,
- (vii) correlation between the spectral index, the reflection amplitude, the width of the iron line and the frequency of the quasi-periodic oscillations.

We show that the multi-zone consideration allows to understand many other observables in the context of the hot flow model:

- (i) hard X-ray lags with logarithmic energy dependence,
- (ii) concave X-ray spectrum,
- (iii) non-thermal OIR excesses and flat spectra,
- (iv) strong correlation between OIR and X-ray emission and a complicated shape of the cross-correlation function,
- (v) a complex evolution of the OIR–UV spectrum during the state transition.

We present relevant analytical equations to estimate the hot flow parameters from the OIR data (see eqs 3, 7 and 6). Additional X-ray and  $\gamma$ -ray data are required to find a complete parameter set. However, the hot flow extent can be found from the OIR data alone under certain assumptions (eqs 11 and 12).

We compare the developed model to the popular jet scenario and show that in a number of cases the data favour the hot flow interpretation. We encourage future observations in the far infrared and submillimeter wavelengths to provide the missing link between radio and infrared, which would allow us to determine the contribution of the two components to the OIR emission.

## ACKNOWLEDGMENTS

The work was supported by the Finnish Graduate School in Astronomy and Space Physics (AV), the Academy of Finland grant 127512 (JP) and ERC Advanced Research Grant 227634 (IV). We

thank Andrzej Zdziarski for fruitful discussions and useful comments and Marion Cadolle Bel for conversations, which helped us to make the paper more understandable.

## REFERENCES

- Akizuki C., Fukue J., 2006, *PASJ*, 58, 469  
 Arévalo P., Uttley P., 2006, *MNRAS*, 367, 801  
 Blandford R. D., Königl A., 1979, *ApJ*, 232, 34  
 Buxton M. M., Bailyn C. D., Capelo H. L., Chatterjee R., Dinçer T., Kalemci E., Tomsick J. A., 2012, *AJ*, 143, 130  
 Cadolle Bel M. et al., 2007, *ApJ*, 659, 549  
 Cadolle Bel M. et al., 2011, *A&A*, 534, A119  
 Casella P. et al., 2010, *MNRAS*, 404, L21  
 Chandrasekhar S., 1960, *Radiative transfer*. Dover, New York  
 Chaty S., Dubus G., Raichoor A., 2011, *A&A*, 529, A3  
 Chaty S., Haswell C. A., Malzac J., Hynes R. I., Shrader C. R., Cui W., 2003, *MNRAS*, 346, 689  
 Chiang C. Y., Done C., Still M., Godet O., 2010, *MNRAS*, 403, 1102  
 Condon J. J., Dressel L. L., 1973, *Ap. Letters*, 15, 203  
 Constantin A., Green P., Aldcroft T., Kim D.-W., Haggard D., Barkhouse W., Anderson S. F., 2009, *ApJ*, 705, 1336  
 Corbel S., Fender R. P., Tzioumis A. K., Nowak M., McIntyre V., Durouchoux P., Sood R., 2000, *A&A*, 359, 251  
 Cunningham C., 1976, *ApJ*, 208, 534  
 de Bruyn A. G., 1976, *A&A*, 52, 439  
 Dermer C. D., Schlickeiser R., 1993, *ApJ*, 416, 458  
 Dinçer T., Kalemci E., Buxton M. M., Bailyn C. D., Tomsick J. A., Corbel S., 2012, *ApJ*, 753, 55  
 Done C., Gierliński M., Kubota A., 2007, *A&ARv*, 15, 1  
 Droulans R., Belmont R., Malzac J., Jourdain E., 2010, *ApJ*, 717, 1022  
 Durant M., Gandhi P., Shahbaz T., Fabian A. P., Miller J., Dhillon V. S., Marsh T. R., 2008, *ApJL*, 682, L45  
 Durant M., Gandhi P., Shahbaz T., Peralta H. H., Dhillon V. S., 2009, *MNRAS*, 392, 309  
 Durant M. et al., 2011, *MNRAS*, 410, 2329  
 Esin A. A., McClintock J. E., Drake J. J., Garcia M. R., Haswell C. A., Hynes R. I., Munro M. P., 2001, *ApJ*, 555, 483  
 Esin A. A., McClintock J. E., Narayan R., 1997, *ApJ*, 489, 865  
 Esin A. A., Narayan R., Cui W., Grove J. E., Zhang S.-N., 1998, *ApJ*, 505, 854  
 Fender R., 2006, in Lewin W., van der Klis M., eds, *Compact stellar X-ray sources*, Cambridge Astrophysics Series, No. 39. Cambridge University Press, Cambridge, p. 381  
 Fender R. P., Belloni T. M., Gallo E., 2004, *MNRAS*, 355, 1105  
 Fender R. P., Garrington S. T., McKay D. J., Muxlow T. W. B., Pooley G. G., Spencer R. E., Stirling A. M., Waltman E. B., 1999, *MNRAS*, 304, 865  
 Fender R. P., Pooley G. G., Brocksopp C., Newell S. J., 1997, *MNRAS*, 290, L65  
 Frank J., King A., Raine D. J., 2002, *Accretion Power in Astrophysics*. Cambridge University Press, Cambridge  
 Frontera F. et al., 2001a, *ApJ*, 546, 1027  
 Frontera F. et al., 2001b, *ApJ*, 561, 1006  
 Gallo E., Migliari S., Markoff S., Tomsick J. A., Bailyn C. D., Berta S., Fender R., Miller-Jones J. C. A., 2007, *ApJ*, 670, 600  
 Gandhi P. et al., 2011, *ApJL*, 740, L13  
 Gandhi P. et al., 2010, *MNRAS*, 407, 2166  
 Gandhi P. et al., 2008, *MNRAS*, 390, L29



- Gelino D. M., Gelino C. R., Harrison T. E., 2010, *ApJ*, 718, 1
- Ghisellini G., Haardt F., Svensson R., 1998, *MNRAS*, 297, 348
- Ghisellini G., Maraschi L., Treves A., 1985, *A&A*, 146, 204
- Gierliński M., Done C., 2003, *MNRAS*, 342, 1083
- Gierliński M., Done C., Page K., 2009, *MNRAS*, 392, 1106
- Gierliński M., Zdziarski A. A., Done C., Johnson W. N., Ebisawa K., Ueda Y., Haardt F., Philips B. F., 1997, *MNRAS*, 288, 958
- Gierliński M., Zdziarski A. A., Poutanen J., Coppi P. S., Ebisawa K., Johnson W. N., 1999, *MNRAS*, 309, 496
- Gilfanov M., 2010, in T. Belloni, ed., *Lecture Notes in Physics*, Vol. 794, Springer Verlag, Berlin, p. 17
- Gilfanov M., Churazov E., Revnivtsev M., 1999, *A&A*, 352, 182
- Gilfanov M., Churazov E., Revnivtsev M., 2000, *MNRAS*, 316, 923
- Ginzburg V. L., Syrovatskii S. I., 1969, *ARA&A*, 7, 375
- Grove J. E., Johnson W. N., Kroeger R. A., McNaron-Brown K., Skibo J. G., Philips B. F., 1998, *ApJ*, 500, 899
- Hannikainen D. C., Hunstead R. W., Campbell-Wilson D., Wu K., McKay D. J., Smits D. P., Sault R. J., 2000, *ApJ*, 540, 521
- Hynes R. I., Bradley C. K., Rupen M., Gallo E., Fender R. P., Casares J., Zurita C., 2009a, *MNRAS*, 399, 2239
- Hynes R. I., Brien K. O., Mullally F., Ashcraft T., 2009b, *MNRAS*, 399, 281
- Hynes R. I., Haswell C. A., Chaty S., Shrader C. R., Cui W., 2002, *MNRAS*, 331, 169
- Hynes R. I. et al., 2003, *MNRAS*, 345, 292
- Hynes R. I., Mauche C. W., Haswell C. A., Shrader C. R., Cui W., Chaty S., 2000, *ApJL*, 539, L37
- Hynes R. I. et al., 2006, *ApJ*, 651, 401
- Ibragimov A., Poutanen J., Gilfanov M., Zdziarski A. A., Shrader C. R., 2005, *MNRAS*, 362, 1435
- Ikejiri Y. et al., 2011, *PASJ*, 63, 639
- Impey C. D., Lawrence C. R., Tapia S., 1991, *ApJ*, 375, 46
- Ingram A., Done C., 2011, *MNRAS*, 415, 2323
- Jourdain E., Roques J. P., Malzac J., 2012, *ApJ*, 744, 64
- Kanbach G., Straubmeier C., Spruit H. C., Belloni T., 2001, *Nature*, 414, 180
- Kato S., Fukue J., Mineshige S., 1998, *Black-hole accretion disks*. Kyoto Univ. Press, Kyoto
- Königl A., 1981, *ApJ*, 243, 700
- Kotov O., Churazov E., Gilfanov M., 2001, *MNRAS*, 327, 799
- Kylafis N. D., Papadakis I. E., Reig P., Giannios D., Pooley G. G., 2008, *A&A*, 489, 481
- Lightman A. P., Shapiro S. L., 1976, *ApJ*, 203, 701
- Ling J. C. et al., 1997, *ApJ*, 484, 375
- Lister M. L., 2001, *ApJ*, 562, 208
- Loskutov V. M., Sobolev V. V., 1981, *Astrofizika*, 17, 535
- Loskutov V. M., Sobolev V. V., 1982, *Astrofizika*, 18, 81
- Lyubarskii Y. E., 1997, *MNRAS*, 292, 679
- Maccarone T. J., Coppi P. S., Poutanen J., 2000, *ApJL*, 537, L107
- Malzac J., Belmont R., 2009, *MNRAS*, 392, 570
- Markoff S., Falcke H., Fender R., 2001, *A&A*, 372, L25
- Marscher A. P., 1977, *ApJ*, 216, 244
- Marscher A. P., Jorstad S. G., Mattox J. R., Wehrle A. E., 2002, *ApJ*, 577, 85
- McClintock J. E. et al., 2001, *ApJ*, 555, 477
- McConnell M. et al., 1994, *ApJ*, 424, 933
- McConnell M. L. et al., 2002, *ApJ*, 572, 984
- Meier D. L., 2005, *ApSS*, 300, 55
- Mirabel I. F., Rodríguez L. F., 1994, *Nature*, 371, 46
- Miyamoto S., Kitamoto S., 1989, *Nature*, 342, 773
- Muno M. P., Mauerhan J., 2006, *ApJL*, 648, L135
- Narayan R., Yi I., 1994, *ApJL*, 428, L13
- Nayakshin S., Melia F., 1998, *ApJS*, 114, 269
- Niedźwiecki A., Xie F.-G., Zdziarski A. A., 2012, *MNRAS*, 420, 1195
- Nolan P. L. et al., 1981, *ApJ*, 246, 494
- Nowak M. A., Vaughan B. A., Wilms J., Dove J. B., Begelman M. C., 1999a, *ApJ*, 510, 874
- Nowak M. A., Wilms J., Dove J. B., 1999b, *ApJ*, 517, 355
- Pacholczyk A. G., Swihart T. L., 1967, *ApJ*, 150, 647
- Pe'er A., Casella P., 2009, *ApJ*, 699, 1919
- Pe'er A., Markoff S., 2012, *ApJ*, 753, 177
- Poutanen J., 1998, in Abramowicz M. A., Björnsson G., Pringle J. E., eds, *Theory of Black Hole Accretion Disks*. Cambridge University Press, Cambridge, p. 100
- Poutanen J., 2001, *Adv. Sp. Res.*, 28, 267
- Poutanen J., 2002, *MNRAS*, 332, 257
- Poutanen J., Coppi P. S., 1998, *Phys. Scr. T*, 77, 57
- Poutanen J., Fabian A. C., 1999, *MNRAS*, 306, L31
- Poutanen J., Krolik J. H., Ryde F., 1997, *MNRAS*, 292, L21
- Poutanen J., Vurm I., 2009, *ApJL*, 690, L97
- Poutanen J., Zdziarski A. A., 2003, in Durouchoux P., Fuchs Y., Rodríguez J., eds, *New Views on Microquasars*. Center for Space Physics, Kolkata, p. 95
- Priedhorsky W., Garmire G. P., Rothschild R., Boldt E., Serlemittos P., Holt S., 1979, *ApJ*, 233, 350
- Quataert E., Narayan R., 1999, *ApJ*, 520, 298
- Rahoui F. et al., 2012, *MNRAS*, 422, 2202
- Revnivtsev M., Gilfanov M., Churazov E., 1999, *A&A*, 347, L23
- Revnivtsev M., Gilfanov M., Churazov E., 2001, *A&A*, 380, 520
- Russell D. M., Fender R. P., 2008, *MNRAS*, 387, 713
- Russell D. M., Fender R. P., 2009, in Wachter A. D., Propst R. J., eds., *Black Holes and Galaxy Formation*. Nova Science Publishers, New York, p. 295
- Russell D. M., Maitra D., Dunn R. J. H., Fender R. P., 2011, *MNRAS*, 416, 2311
- Rybicki G. B., Lightman A. P., 1979, *Radiative processes in astrophysics*. New York, Wiley-Interscience
- Schultz J., Hakala P., Huovelin J., 2004, *Baltic Astronomy*, 13, 581
- Shadmehri M., Khajenabi F., 2005, *MNRAS*, 361, 719
- Shahbaz T., Fender R. P., Watson C. A., O'Brien K., 2008, *ApJ*, 672, 510
- Shakura N. I., Sunyaev R. A., 1973, *A&A*, 24, 337
- Shidatsu M. et al., 2011, *PASJ*, 63, 785
- Sikora M., Begelman M. C., Rees M. J., 1994, *ApJ*, 421, 153
- Sobolev V. V., 1963, *A treatise on radiative transfer*. Van Nostrand, Princeton
- Sobolewska M. A., Papadakis I. E., Done C., Malzac J., 2011, *MNRAS*, 417, 280
- Soleri P. et al., 2010, *MNRAS*, 406, 1471
- Stern B. E., Poutanen J., 2006, *MNRAS*, 372, 1217
- Veledina A., Poutanen J., Vurm I., 2011a, *ApJL*, 737, L17
- Veledina A., Vurm I., Poutanen J., 2011b, *MNRAS*, 414, 3330
- Vurm I., Poutanen J., 2009, *ApJ*, 698, 293
- Wardziński G., Zdziarski A. A., 2000, *MNRAS*, 314, 183
- Wardziński G., Zdziarski A. A., 2001, *MNRAS*, 325, 963
- Weisskopf M. C., Silver E. H., Kestenbaum H. L., Long K. S., Novick R., Wolff R. S., 1977, *ApJL*, 215, L65
- Wills B. J., Wills D., Evans, II N. J., Natta A., Thompson K. L., Breger M., Sitko M. L., 1992, *ApJ*, 400, 96
- Yan Z., Yu W., 2012, *MNRAS*, in press, arXiv:1104.2785

- Zdziarski A. A., Gierliński M., 2004, *Progress of Theoretical Physics Supplement*, 155, 99
- Zdziarski A. A., Gierliński M., Mikołajewska J., Wardziński G., Smith D. M., Harmon B. A., Kitamoto S., 2004, *MNRAS*, 351, 791
- Zdziarski A. A., Grove J. E., Poutanen J., Rao A. R., Vadawale S. V., 2001, *ApJL*, 554, L45
- Zdziarski A. A., Lubiński P., Gilfanov M., Revnivtsev M., 2003, *MNRAS*, 342, 355
- Zdziarski A. A., Lubiński P., Sikora M., 2012, *MNRAS*, 423, 663
- Zdziarski A. A., Lubinski P., Smith D. A., 1999, *MNRAS*, 303, L11
- Zdziarski A. A., Poutanen J., Mikołajewska J., Gierliński M., Ebisawa K., Johnson W. N., 1998, *MNRAS*, 301, 435
- Zdziarski A. A., Poutanen J., Paciesas W. S., Wen L., 2002, *ApJ*, 578, 357

$$t_{\text{adv}} \approx 20 \sqrt{\frac{R^3}{GM}}. \quad (\text{A5})$$

We can compare the Coulomb (the radiative cooling is faster than Coulomb for  $R \leq 100R_S$ ) and advection time-scales (again, assuming  $\bar{\gamma}_{\text{eq}} = 1$ )

$$\frac{t_{\text{cool,Coul}}}{t_{\text{adv}}} \approx 5 \times 10^{-4} \frac{\gamma}{\tau} \left( \frac{R}{10R_S} \right)^{-1/2}. \quad (\text{A6})$$

Hence, for typical parameters  $\gamma \sim 1$ –100 and  $\tau \sim 0.1$ –1 the cooling time-scale is shorter than the advection time.

## APPENDIX A: TYPICAL TIME-SCALES

### A1 Radiative versus Coulomb time-scales

The synchrotron cooling time can be calculated as (e.g. Rybicki & Lightman 1979)

$$t_{\text{cool,s}} = \frac{\gamma - 1}{|\dot{\gamma}_s|} = \frac{1}{\gamma + 1} \left( \frac{4}{3} \frac{\sigma_T U_B}{m_e c} \right)^{-1}, \quad (\text{A1})$$

where  $\dot{\gamma}_s$  is synchrotron cooling rate. The cooling time for Compton scattering is similar. After a little algebra one can obtain

$$t_{\text{cool,s}} \approx \frac{7.5 \times 10^{-4}}{\gamma + 1} \frac{R}{c \eta_B} \left( \frac{L}{L_{\text{Edd}}} \right)^{-1} \left( \frac{R}{10R_S} \right), \quad (\text{A2})$$

where  $\eta_B = 3U_B/(4\pi U_{\text{rad}})$  denotes the ratio of the magnetic and radiation field energy densities. The typical time-scale of e-e Coulomb energy exchange at the equilibrium can be estimated as (e.g. Nayakshin & Melia 1998)

$$t_{\text{cool,Coul}} = \frac{\gamma - 1}{|\dot{\gamma}_{\text{Coul}}|} \approx \frac{2R}{3c} \frac{\bar{\gamma}_{\text{eq}}}{\tau \ln \Lambda} \frac{z^3}{\gamma(\gamma + 1)}, \quad (\text{A3})$$

where  $z$  is the particle momentum in units of  $m_e c$ ,  $\bar{\gamma}_{\text{eq}}$  is the average Lorentz factor of the electrons in equilibrium and  $\ln \Lambda$  is the Coulomb logarithm. At higher Lorentz factors the cooling is determined by radiative processes, while for lower  $\gamma$  the non-radiative Coulomb collisions are dominant. The relative role of radiative and Coulomb cooling changes with radius:

$$\frac{t_{\text{cool,Coul}}}{t_{\text{cool,s}}} \approx 56 \frac{z^3 \eta_B}{\gamma \tau} \left( \frac{L}{L_{\text{Edd}}} \right) \left( \frac{R}{10R_S} \right)^{-1}, \quad (\text{A4})$$

where we used  $\bar{\gamma}_{\text{eq}} = 1$  and  $\ln \Lambda = 17$ . Therefore, the Coulomb exchange rates start dominating over the radiative cooling with an increasing size.

### A2 Coulomb versus accretion time-scales

We assume the spectra and electron distributions in each zone are in equilibrium, thus the typical time-scales of equilibration should be much less than the dynamical time-scale at a given distance. To estimate the latter, we consider the properties of an ADAF flow, derived by Narayan & Yi (1994). Taking their radial velocity approximation, viscosity parameter 0.1 and assuming the adiabatic index 3/2 (Quataert & Narayan 1999), we obtain the advection/accretion time